2013

A Laboratory Experiment Using Nanoindentation to Demonstrate the Indentation Size Effect

Wendelin Wright
Bucknell University, wendelin@bucknell.edu

Gang Feng
Villanova University, gang.feng@villanova.edu

William D. Nix
Stanford University, nix@stanford.edu

Recommended Citation
Wright, Wendelin; Feng, Gang; and Nix, William D.. "A Laboratory Experiment Using Nanoindentation to Demonstrate the Indentation Size Effect." *Journal of Materials Education* 35, no. 5-6 (2013) : 135-144.

Journal of Materials Education Vol.35 (5-6): 135 - 144 (2013)

A LABORATORY EXPERIMENT USING NANOINDENTATION TO DEMONSTRATE THE INDENTATION SIZE EFFECT

Wendelin J. Wright[1], G. Feng[2] and W.D. Nix[3]

[1]Departments of Mechanical Engineering and Chemical Engineering, Bucknell University, One Dent Drive, Lewisburg, PA 17837; *wendelin@bucknell.edu* ;
[2]Department of Mechanical Engineering, Villanova University, 800 Lancaster Avenue, Villanova, PA 19085; *gang.feng@villanova.edu* ;
[3]Department of Materials Science and Engineering, Stanford University, 496 Lomita Mall, Stanford, CA 94305; *nix@stanford.edu*

ABSTRACT

A laboratory experiment using nanoindentation to demonstrate the indentation size effect is described. This laboratory introduces students to sophisticated instrumentation at low cost and low risk and utilizes recent research in the materials community as its foundation. The motivation, learning objectives, experimental details, data, and data analysis are presented. This experiment is intended for use in an upper-division materials science elective at the university level and has been successfully used in laboratory courses for senior undergraduates and first-year graduate students at Stanford University and Santa Clara University.

Keywords: *nanoindentation laboratory, indentation size effect, dislocations*

INTRODUCTION

A nanoindenter is an instrument that presses a small tip into the material of interest and measures the applied load and imposed displacement with micro-newton and sub-nanometer resolution, respectively. A schematic diagram of a nanoindenter is shown in Figure 1. Mechanical properties such as elastic modulus and hardness are obtained from the load and displacement data. Critical developments related to the analysis of nanoindentation data occurred in the 1980s[1–3], and nanoindentation continues to be an important experimental tool for analyzing the mechanical properties of materials at small length scales. Nano-indentation was originally developed to study the elastic modulus and hardness of hard materials such as thin metal films, but today it is widely used for studying the behavior of viscoelastic materials[4–8], biological materials[9], and micro- and nanostructures such as beams[10] and pillars[11]. Nanoindenters have also been incorporated into transmission electron microscopes for in-situ studies of the relationship between microstructure and

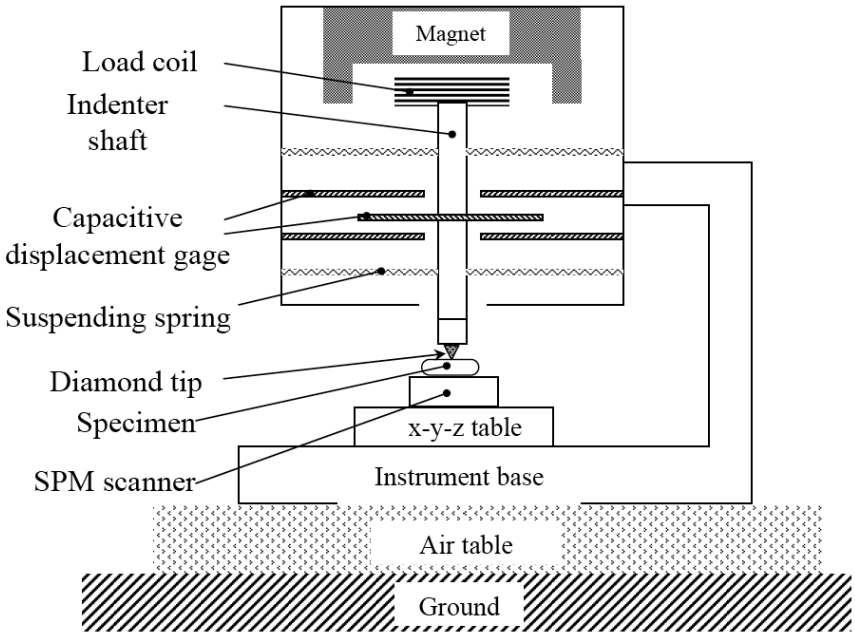

Figure 1. A schematic diagram of a nanoindenter that uses a load coil to impose the load and capacitive gages to measure the displacement. The indenter shaft is supported by springs. A scanning probe microscope (SPM) is sometimes included to facilitate imaging of the material before and after indentation.

deformation[12]. Several reviews of the nanoindentation literature have been presented recently[12–15]. Applications include determination of mechanical properties for thin film materials used in integrated circuit components, hard or corrosion-resistant coatings for cutting tools, structures such as nanowires and micropillars, and bone.

The indentation size effect is the focus of this materials science laboratory experiment, which illustrates how materials behavior, and in particular mechanical behavior, may change at small length scales. This concept is critical to applications such as micro- and nanoelectronics where the characteristic length scales of devices are such that differences in materials properties from the bulk counterparts are often observed (e.g., the strengths of materials at small length scales are typically higher). The indentation size effect is demonstrated in a single crystal using nanoindentation. This experiment follows the treatments of Nix and Gao[16] and Feng and Nix[17]. It is appropriate for use in an upper-division undergraduate materials science elective at an institution with laboratory instrumentation that includes a nanoindenter.

By analyzing the hardness of a single crystal as a function of indentation depth, students investigate the indentation size effect, the phenomenon that the hardness of crystalline materials at indentation depths on the order of 1 μm or less is higher than hardness measured at larger depths. The indentation size effect is the consequence of strain gradient plasticity[18]; during nanoindentation of a crystalline material, dislocations must be created to accommodate the shape change imposed by the indenter at small length scales[16] as shown in Figure 2. These so-called geometrically necessary dislocations exist in addition to the statistically stored dislocation density and lead to the hardening that manifests as the indentation size effect. At indentation depths larger than 1 μm, the geometrically necessary dislocation density is generally negligible compared to the statistically stored dislocation density and the indentation size effect is not observed. The statistically stored dislocations are those that

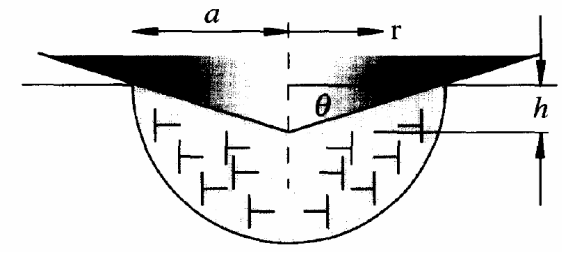

Figure 2. A diagram of the geometrically necessary dislocations created by a rigid conical indentation with contact radius a, dislocation loop radius r, depth of indentation h, and angle θ between the surface of the conical indenter and the plane of the surface as presented by Nix and Gao[16]. Reprinted with permission. Copyright 2008, Elsevier.

exist due to homogeneous strain, and their density is not expected to change with indentation depth.

In this experiment, students are able to observe the transition from elastic to plastic deformation and witness the effects of dislocation activity in real time. This laboratory provides an opportunity to introduce students to sophisticated instrumentation at low cost and low risk and utilizes recent research in the materials community as its foundation. The use of curve fits is emphasized in the data analysis. The learning objectives of this experiment are to

1) understand one mechanism by which the mechanical properties of materials at small length scales may be different from bulk values (i.e., the indentation size effect);
2) gain familiarity with the experimental technique of nanoindentation;
3) interpret hardness data as a function of indentation depth;
4) observe effects of dislocation activity; and
5) use linear curve fitting to extract model parameters.

The background theory, experimental details, data, and data analysis are presented in the sections that follow.

THE INDENTATION SIZE EFFECT

The Nix and Gao[16] model for the indentation size effect states that hardness H increases significantly with small indentations according to

$$H^2 = H_0^2\left(1+\frac{h_0}{h}\right), \qquad (1)$$

where H_0 is the hardness when the indentation depth h becomes infinitely large and h_0 is a length scale that depends on the indenter shape, the shear modulus, and H_0. If H_0 is treated as a constant, a plot of H^2 as a function of the ratio $1/h$ should give a linear function with an intercept at $\frac{1}{h}=0$ equal to H_0^2 and a slope equal to $H_0^2 h_0$. By first determining H_0^2, h_0 can be calculated from the slope value. Equation (1) is the fundamental principle underlying the motivation for this experiment. It follows from the Taylor relationship, which states that the strength of a crystal is directly proportional to the square root of the total dislocation density; the proportionality between strength and hardness; and the geometry of the indentation[16]. For a derivation of Equation (1), see the reference from Nix and Gao[16].

NANOINDENTATION

The following brief description of nanoindentation is presented for those instructors who may be unfamiliar with the technique. This description follows the Oliver and Pharr method of analysis[3,13].

During nanoindentation, a sharp indenter is pressed into an initially undeformed surface, and the load P is measured as a function of indentation depth h. Elastic modulus and hardness can be extracted from indentation data. Indenter tips are available in a variety of geometries. One of the most commonly used geometries is that of a Berkovich indenter, which is a three-sided pyramid. The projected contact area A_c under load for a perfect Berkovich indenter is given by

$$A_c = 24.5h_c^2, \qquad (2)$$

where h_c is the contact depth. Equation (2)

relates the cross-sectional area of the indenter to the distance from the tip. In practice, indenters are not perfect, and each tip must be calibrated to determine its area function $A_c = f(h_c)$ by first indenting into a material of known elastic properties such as fused silica. A function of the following form is typically used for a Berkovich indenter:

$$A_c(h_c) = 24.5\,h_c^2 + C_1 h_c + C_2 h_c^{1/2} + C_3 h_c^{1/4} + \ldots\ldots + C_8 h_c^{1/128} \quad (3)$$

where the C_i terms are constants determined by curve fitting procedures. The higher order terms correct for defects at the tip, whereas the leading term dominates at larger depths of indentation. See Figure 3 for a schematic diagram of an imperfect Berkovich indenter illustrating the relationship between h_c and A_c.

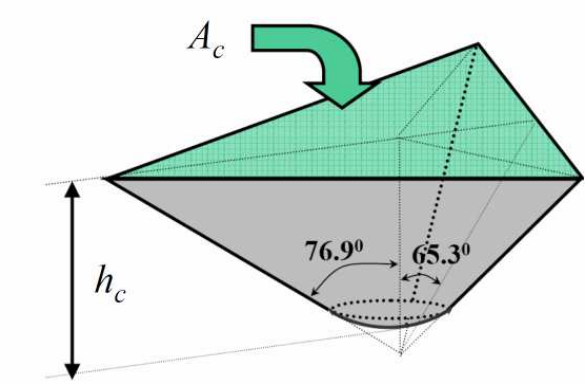

Figure 3. A schematic diagram illustrating the relationship between the contact depth h_c and the contact area A_c .

Figure 4 shows a typical plot of load P versus depth of indentation h for a sharp indenter. On loading to a depth of h_{max}, the deformation is both elastic and plastic due to the sharpness of the indenter tip. In general, on unloading, the deformation is purely elastic and follows a power law relation given by

$$P = \alpha\left(h - h_f\right)^m, \quad (4)$$

where α and m are constants and h_f is the depth of the residual impression. These three constants are determined by a least squares fitting procedure. The initial slope during unloading is the stiffness $S = dP/dh$. Thus,

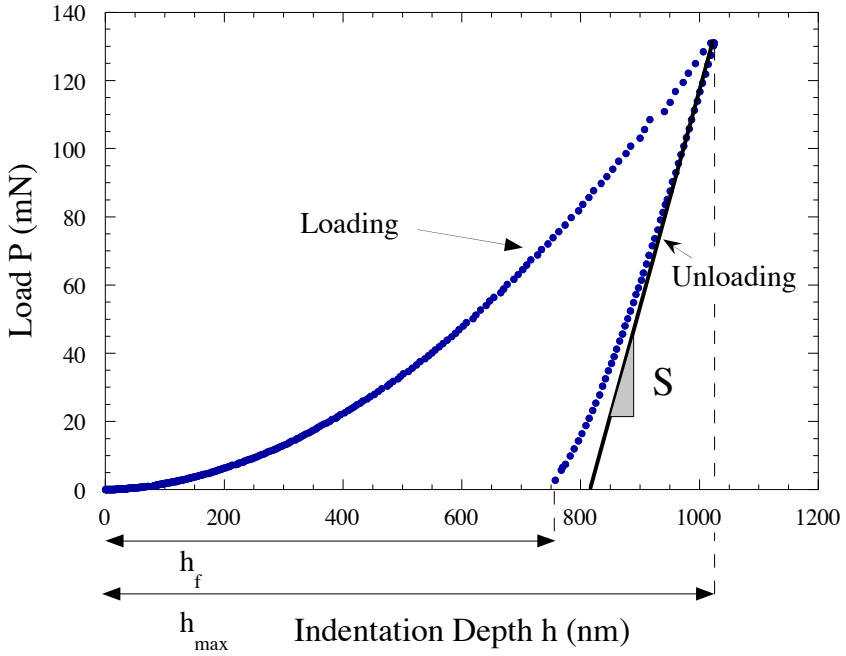

Figure 4. Typical load P as a function of depth h for indentation with a sharp indenter illustrating the depth of the residual hardness impression h_f, the maximum indentation depth h_{max}, and the unloading stiffness S.

the unloading stiffness is found by differentiating Equation (4) with respect to h and evaluating S at h_{max}.

During indentation, sink-in at the periphery of the indentation means that the total indentation depth as measured by the displacement of the tip is the sum of the contact depth and the depth h_s at the periphery of the indentation where the indenter does not make contact with the material surface, i.e.,

$$h = h_c + h_s . \tag{5}$$

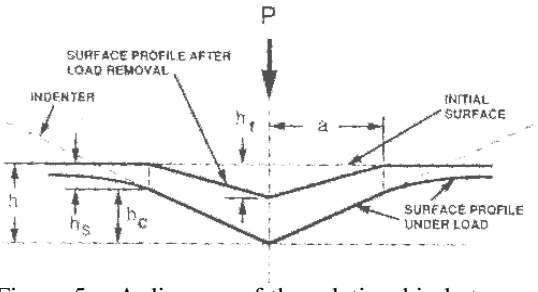

Figure 5. A diagram of the relationship between h, h_c, and h_s as presented by Oliver and Pharr[3]. Reprinted with permission. Copyright 1992, Cambridge University Press.

Figure 5 shows a diagram of the relationship between h, h_c, and h_s as presented by Oliver and Pharr[3]. The surface displacement term h_s can be calculated according to

$$h_s = \varepsilon \frac{P_{max}}{S}, \tag{6}$$

where P_{max} is the load at maximum depth and ε is a geometric constant equal to 0.75 for a Berkovich indenter. Once h_c is known (such that A_c is known), the reduced modulus E_r can be calculated according to

$$E_r = \frac{\sqrt{\pi}}{2\beta} \frac{S}{\sqrt{A_c}}, \tag{7}$$

where β is a correction factor that accounts for the lack of axial symmetry for pyramidal indenters. For the Berkovich indenter, the constant $\beta = 1.034$. The reduced modulus E_r accounts for the effects of the non-rigid indenter and is given by

$$\frac{1}{E_r} = \frac{1-\nu^2}{E} + \frac{1-\nu_i^2}{E_i}, \tag{8}$$

where ν and E are the Poisson's ratio and elastic modulus of the material being indented, and ν_i and E_i are the Poisson's ratio and elastic modulus of the indenter.

The hardness H is calculated according to

$$H = \frac{P_{max}}{A_c}, \tag{9}$$

where again P_{max} is the maximum indentation load and A_c is the projected contact area under load between the indenter and the material being indented as determined using the tip shape function of Equation (3). Hardness as determined by nanoindentation is typically reported with units of GPa.

The hardness H and elastic modulus E as determined by Equations (3)–(9) are now known as the Oliver and Pharr hardness and modulus after Warren C. Oliver and George M. Pharr[3]. Alternatively, the depth profiles of hardness and modulus can be determined by the continuous measurement of contact stiffness as a function of indentation depth. This is a dynamic technique in which a small oscillating load is superimposed on the total load on the sample. The corresponding oscillating displacement and the phase angle between the load and displacement are measured. In practice, most commercial nanoindentation platforms will automatically compute the elastic modulus and hardness as a function of indentation depth once the tip shape calibration is known.

If a single crystal is initially dislocation free, the transition from elastic to plastic deformation can be observed during the preliminary stage of indentation. At shallow indentation depths, the blunt tip of the indenter can be modeled as a sphere with a radius of curvature R determined from a tip shape calibration. For purely elastic contacts, the indenting load P can be related to the indenter displacement h using the Hertz theory of normal contact between two frictionless elastic solids[19]:

$$P^{\frac{2}{3}} = \left(\frac{4}{3} E_r \sqrt{R}\right)^{\frac{2}{3}} h \,. \qquad (10)$$

Equation (10) can be used for a variety of purposes. For example, if the reduced modulus is known, a plot of $P^{2/3}$ versus h can be fit to determine the radius R of the indenter, or if R is known, E_r can be determined from a plot of $P^{2/3}$ versus h. Clear deviations from the elastic behavior mark a transition from elastic to plastic deformation. In a crystalline material, sudden increases in displacement at this transition are attributed to dislocation nucleation and commonly also dislocation multiplication events and are typically referred to as "pop-ins." A pop-in in MgO is shown in Figure 6.

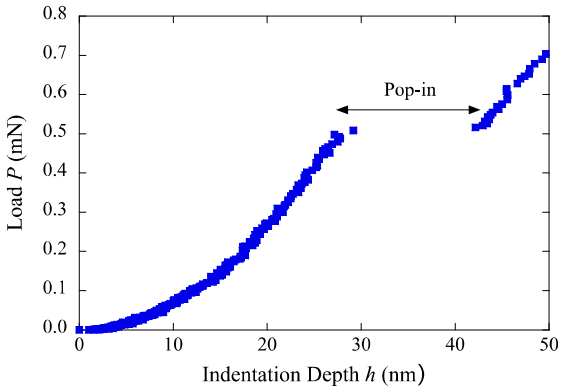

Figure 6. Load as a function of indentation depth for a single indentation of MgO. A pop-in is clearly visible.

EXPERIMENTAL DETAILS

A minimum of twelve indentations should be performed on fused silica using a Berkovich tip to an indentation depth of 1.0 μm and averaged to generate the tip shape calibration. Twelve indents balance time efficiency with a sufficient amount of data. Commercial nanoindentation platforms typically perform the calibration automatically based on the calibration data and a few inputs from the user such as the type of tip being used and its elastic constants, the elastic constants of the calibration material, and the number of parameters to be used in the fit of Equation (3) The elastic moduli of diamond and fused silica are 1.141 TPa and 72 GPa, respectively; the respective Poisson's ratios are 0.07 and 0.17. For this experiment, an appropriate number of fitting parameters is five. The tip shape calibration is then applied to the same tip to depths of 1.0 μm on the specimen of interest. We have chosen to use polished single crystal (100) MgO ($\nu = 0.17$) because it clearly demonstrates the indentation size effect[17]. Also epi-polished (100) MgO substrates can be purchased from a variety of vendors at reasonable cost. Note that the MgO should be stored in a desiccator to prevent the formation of a surface layer (due to reaction with water in the air) that would suppress pop-in formation. Other single crystal materials such as copper or silver may be used instead of MgO to observe the indentation size effect[16]. The specimen must be a single crystal and ideally should be electro polished as a final processing step to remove mechanical damage from the polishing process. A constant load rate to load ratio $\dot{P}/P$ of 0.05 s^{-1} is recommended for indentations on both materials. If the load and displacement data for the indentations are observed in real-time, the pop-ins in MgO should be visible in the data as they occur. Blunter tips such as spherical and conical tips with large radii of curvature promote pop-in formation. A Berkovich tip is used here for convenience. The initial radius of curvature of a tip is specified by the manufacturer for all tip shapes, but the tip will likely become blunter with use. The ASM Handbook provides a helpful summary of indentation procedures[20].

STUDENT WORK

In prior offerings of this laboratory exercise, students performed the experiment and analyzed the data in groups of three and subsequently wrote individual reports in the format of standard journal articles. A suggestion for future improvement would be to analyze the data on a class-wide basis to assess experimental variability and uncertainty.

The following instructions are offered as suggestions for student laboratory reports. Results for these items will be presented in the next section.

1. Plot the elastic modulus of fused silica and MgO as a function of indentation depth. Describe the features of the elastic modulus plots. Does the modulus of MgO have the expected value of 288 GPa?
2. Determine the radius of the indenter tip using the data for MgO at small indentation depths (less than the depth at which the pop-ins in MgO occur). Show a magnification of the elastic loading (P versus h and also $P^{2/3}$ versus h) of MgO at small indentation depths. Fit the $P^{2/3}$ versus h data at small indentation depths with the Hertz theory, and based on the elastic modulus of MgO, determine the equivalent radius of the indenter tip. Comment on the meaning of the sudden increment of displacement and the change in slope of the $P^{2/3}$ versus h plot for MgO.
3. Plot the hardness of MgO as a function of indentation depth.
4. Plot H^2 as a function of $1/h$ for MgO. Determine the values of H_0 and h_0 with a linear fit to the data. Comment on the significance of the trends in the plot with respect to the indentation size effect. Is H_0 consistent with the values of H at large indentation depths?

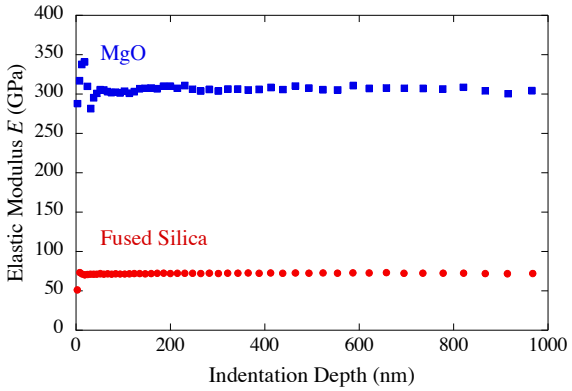

Figure 7. The elastic modulus of fused silica and MgO as a function of indentation depth.

RESULTS AND ANALYSIS

Figure 7 is a plot of the elastic modulus of fused silica and MgO as a function of indentation depth based on the averaged results for valid indentations for each material (twelve indents for each material as performed by a single group). The elastic modulus for both materials should be constant with indentation depth. If a varying elastic modulus for MgO is observed, this trend is likely due to an error in the calibration of the machine stiffness; an experienced nanoindentation user should be consulted to address this issue that can arise when indenting stiff materials such as MgO. According to Figure 7, MgO has an average elastic modulus of 306.5 +/– 2.9 GPa, compared to the expected value of 288 GPa. This difference of 6% between the theoretical and measured values is considered to be good agreement.

Figure 6 shows the load-displacement curve for a single representative indentation into MgO, indicating a dislocation nucleation event and the onset of plastic behavior. (Note that data for pop-in events should be obtained from a single indentation rather than averaged over many indentations since this behavior is discrete.) A dislocation nucleation event such as this is immediately visible in a plot of load versus indentation depth when such plots are provided by real-time displays of commercial nanoindentation platforms. Fused silica does not show this behavior because it is amorphous (i.e., it does not have dislocations). (Note that the load and displacement values at which pop-ins occur will vary with the radius of curvature of the tip and the surface quality of the sample. For sharper tips, the load and displacement values at which pop-ins occur will be lower than the values observed for blunter tips.) Figure 8 is a plot of $P^{2/3}$ versus h for the representative indentation into MgO shown in Figure 6. By performing a linear fit to the data before the pop-in event, the radius of the tip (which is modeled as a sphere) is estimated to be 122 nm according to Equation (10) and the measured reduced modulus of 248 GPa for

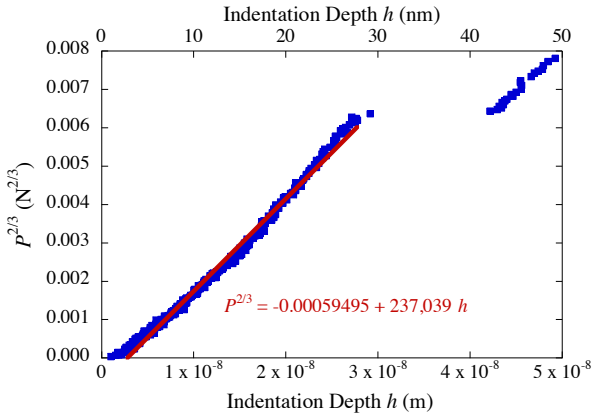

Figure 8. $P^{2/3}$ versus h for the indentation shown in Fig. 6. The equivalent radius of the indenter tip is determined to be 122 nm from the linear fit and Equation (10). The curve fit shown uses the lower horizontal axis with units of meters.

MgO. The fit is only valid to a load of approximately 0.5 mN and a total indentation depth of approximately 28 nm as these are the values at which the pop-in occurs.

Figure 9 is a plot of the hardness of MgO as a function of indentation depth. The increase in hardness at small depths of indentation is the manifestation of the indentation size effect. Figure 10 is a plot of H^2 as a function of $1/h$ for MgO. Using a linear fit to the data and Equation (1), H_0 is determined to be 9.1 GPa (consistent with the hardness at large indentation depths), and h_0 is determined to be 91 nm. For an analytical expression for h_0, see the paper by Nix and Gao[16]. It should be noted

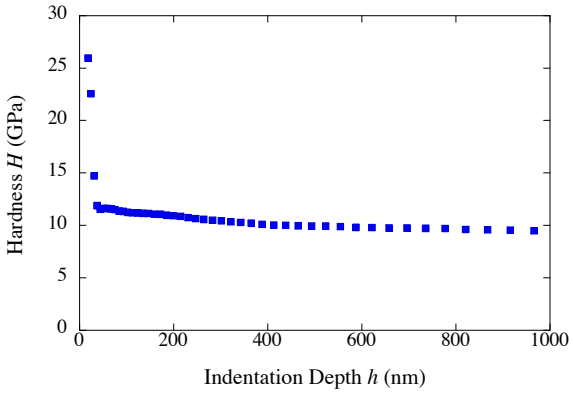

Figure 9. Hardness as a function of indentation depth for MgO.

that H^2 deviates from the linear relation for $1/h > 0.005$ nm^{-1}, i.e., $h < 200$ nm. Two possible reasons for this deviation *at the small indentation depths* are (1) the ratio between the effective radius of the indentation plastic zone and the radius of contact between the indenter and the specimen surface is not constant[17] and (2) the oscillating displacement for the continuous stiffness measurement is significant compared to the total elastically recoverable displacement[21]. The first reason dominates the behavior seen here since the calculated modulus of MgO is still constant in the range of $h < 200$ nm (see Figure 7); otherwise, the modulus would decrease with decreasing h due to the second reason. Note that the hardnesses shown in Figures 9 and 10 are the averaged results for all valid indentations from a single student group for each material.

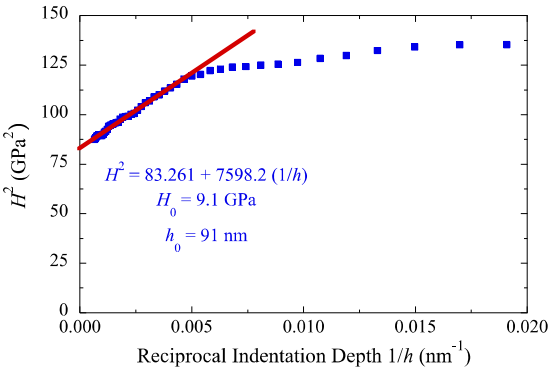

Figure 10. H^2 as a function of $1/h$ for MgO.

This experiment has been performed successfully in laboratory courses for senior undergraduates and first-year graduate students at Stanford University and Santa Clara University. Instructor observation of the students in the laboratory sessions and review of the student laboratory reports indicate that the learning objectives were met. No changes to the experiment were proposed based on the first two offerings.

SUMMARY

A laboratory experiment to determine the indentation size effect in (100) MgO using nanoindentation has been presented. Suggested

discussion points for student reports and typical results have been included for instructor use. The discrete nature of dislocation activity is highlighted as is the importance of differences in mechanical behavior from the bulk at small length scales. A related student exercise would involve etching the (100) MgO substrate to observe the pattern of dislocation etch pits that form on the surface using scanning electron microscopy. Details of the etch pitch procedure are available in the article by Feng and Nix[17].

REFERENCES

1. M.F. Doerner and W.D. Nix, *J. Mater. Res.* **1**, 601 (1986).
2. J.B. Pethica and W.C. Oliver, in J.C. Bravman, W.D. Nix, D.M. Barnett, and D.A. Smith (eds.): *Thin Films: Stresses and Mechanical Properties*, Materials Research Society Symposium Proceedings, Materials Research Society, Warrendale, PA, USA, **130**, 13 (1989).
3. W.C. Oliver and G.M. Pharr, *J. Mater. Res.* **7(6)**, 1564 (1992).
4. C.C. White, M.R. Vanlandingham, P.L. Drzal, N-K. Chang, and S-H. Chang, *J. Polym. Sci: Part B: Polym. Phys.*, **43(14)**, 1812 (2005).
5. E.G. Herbert, W.C. Oliver, and G.M. Pharr, *J. Phys. D: Appl. Phys.* **41(7)**, 074021 (2008).
6. E.G. Herbert, W.C. Oliver, A. Lumsdaine, and G.M. Pharr, *J. Mater. Res.* **24(3)**, 626 (2009).
7. W.J. Wright and W.D. Nix, *J. Mater Res.* **24(3)**, 863 (2009).
8. W.J. Wright, A.R. Maloney, and W.D. Nix, *Int. J. Surface Sci. Eng.,* **1(2–3)** 274 (2007).
9. M.L. Oyen, *Exp. Techniques* **37(1)**, 73 (2013).
10. T.P. Weihs, S. Hong, J.C. Bravman, and W.D. Nix, *J. Mater. Res.* **3(5)**, 931 (1988).
11. M.D. Uchic, D.M. Dimiduk, J.N. Florando, and W.D. Nix, *Science,* **305(5686)**, 986 (2004).
12. H. Nili, K. Kalantar-zadeh, M. Bhaskaran, and S. Sriram. *Prog. Mat. Sci.* **58**, 1 (2013).
13. W.C. Oliver and G.M. Pharr, *J. Mater. Res.* **19(1)**, 3 (2004).
14. L.D. Marks, O.L. Warren, A.M. Minor, and A.P. Merkle. *MRS Bulletin* **33**, 1168 (2008).
15. W.C. Oliver and G.M. Pharr, *MRS Bulletin* **35**, 897 (2010).
16. W.D. Nix and H. Gao, *J. Mech. Phys. Solids* **46**, 411 (1998).
17. G. Feng and W.D. Nix, *Scripta Mater.* **51**, 599 (2004).
18. M.F. Ashby, *Phil. Mag.* **21**, 399 (1970).
19. K. L. Johnson, *Contact Mechanics*, Cambridge University Press, Cambridge, (1985)., pp. 93 and 62
20. J.L. Hay and G.M. Pharr, in *ASM Handbook Volume 8, Mechanical Testing and Evaluation,* ASM International, Materials Park, OH, USA (2000), p. 231.
21. G.M. Pharr, J.H. Strader, and W.C. Oliver, *J. Mater. Res.* **24(3)**, 653 (2009).

This page intentionally left blank